The current issue and full text archive of this journal is available at
www.emeraldinsight.com/0961-5539.htm

Analysing an adaptive finite volume for flow in highly heterogeneous porous medium

Sanjay Kumar Khattri
Stord/Haugesund University College, Haugesund, Norway

Received 31 July 2006
Revised 15 March 2007
Accepted 15 March 2007

Abstract

Purpose – This paper seeks to develop an adaptive finite volume algorithm, and to present an extensive numerical analysis of it.

Design/methodology/approach – The effectiveness of the developed algorithm is demonstrated through practical and computationally challenging problems. The algorithm is tested for a wide range of singularities.

Findings – The convergence of the presented algorithm is independent of the regularity of the problems. It is shown that the our algorithm produces more accurate and well conditioned matrix systems.

Research limitations/implications – Though the presented algorithm works for extreme singularities on rectangular meshes, it may not be as efficient if the underlying meshes are distorted, and it may not converge. Further research is under way for including the multi-point approximation technique into the algorithm.

Practical implications – Almost all reservoir simulators use the two-point method, and this algorithm is based on this method. The algorithm can be easily incorporated into the reservoir simulators. The results show that such an implementation will greatly improve the computational efficiency of the simulators. The work is useful for computational scientists, and especially for the researchers in oil industries. The paper reports the numerical work with practical applications.

Originality/value – The paper develops an adaptive finite volume algorithm. It is shown that adaptive meshes represent the underlying problem more accurately, and matrix systems associated with adaptive meshes are easier to solve compared with matrix systems associated with uniform meshes.

Keywords Finite volume methods, Porous materials, Numerical analysis

Paper type Research paper

1. Introduction

Owing to reasons of simplicity and computational efficiency, the two-point flux approximation (TPFA) or the 2-point finite volume method (2P-FVM) is most widely used method for understanding fluid flow in porous media. For example, Exxon Mobil Corporation's reservoir simulator EM$^{\text{power}^{TM}}$ (Wu and Parashkevov, 2005), Schlumberger's Eclipse (1997), the general purpose research simulator at the Stanford University (Cao, 2002), the research simulator at the Norsk Hydro (Hydro, 2001), the research simulator at the Chevron Texaco (Lee *et al.*, 1999), the research simulators at the University of Bergen (Garrido *et al.*, 2004) and the well known numerical simulator TOUGH-2 at the Lawrence

The author thanks Ivar Aavatsmark for providing useful comments, and Many L. Buddle and David R. Wood for correcting the manuscript.

International Journal of Numerical Methods for Heat & Fluid Flow
Vol. 18 No. 2, 2008
pp. 237-257

0961-5539
DOI 10.1108/09615530810846365

Berkeley National Laboratory for capturing dynamics of green house gases in porous medium (Pruess *et al.*, 2002). All of these simulators use the 2P-FVM on uniform meshes.

Many problems such as multi-component, multi-phase flow and flow in heterogenous porous media result in singular or localised solutions. These problems have many practical implications. For example, storage of green house gases in aquifers, hydrocarbon flow in reservoirs and ground water remediation. It is well known that the 2P-FVM on uniform meshes is not an effective technique for capturing singular solutions (Eigestad and Klausen, 2005). Convergence rate of the 2P-FVM on uniform meshes depends on the regularity of the solution.

We present 2P-FVM on adaptive meshes. Through numerical work, we show that the convergence of the presented adaptive technique does not depend on the regularity or the singularity of the solution. The adaptive technique depends on several factors such as, error indicator and adaptive algorithm. We present a simple adaptive criterion, an adaptive algorithm and several examples.

There are several advantages to our technique. The adaptive technique can be easily implemented in existing simulators because we do not change the discretization method (flux across internal edges is given by the TPFA). Another advantage of our scheme is it results in symmetric and positive definite matrix systems, so efficient solvers such as the conjugate gradient (CG) can be used. In addition to simple and fast, other big advantage of the two-point discretization is that the matrix system associated with it is always monotone (Nordbotten and Eigestad, 2005). It is important to point out that ensuring monotonicity of a discretization technique is difficult (Nordbotten and Eigestad, 2005) and non-monotone schemes can provide unphysical results (Aavatsmark, 2002; Nordbotten and Eigestad, 2005). For convergence of the 2P-FVM on uniform, locally refined and non-uniform meshes, the following works are recommended (Ewing *et al.*, 1991a, b; Forsyth and Sammon, 1988; Süli, 1991; Weiser and Wheeler, 1988). A numerical analysis of the convergence of the 2P-FVM on uniform meshes can be found in Eigestad and Klausen (2005).

Now let us consider the steady state pressure equation of a single phase flowing in a porous medium Ω:

$$-\mathrm{div}(\mathbf{K}\,\mathrm{grad}\,p) = f \quad \text{in} \quad \Omega, \tag{1}$$

$$p(x,y) = p^D \quad \text{on} \quad \partial\Omega_D. \tag{2}$$

Here, Ω is a polyhedral domain in $\mathbb{R}^2$, the source function f is assumed to be in $L^2(\Omega)$ and the diagonal tensor coefficient $\mathbf{K}(x,y)$ is positive definite and piecewise constant. $\mathbf{K}$ is allowed to be discontinuous in space. In porous media flow (Aziz and Settari, 1979; Aavatsmark, 2002; Eigestad and Klausen, 2005; Nordbotten and Eigestad, 2005), the unknown function $p = p(x,y)$ represents the pressure of a single phase, $\mathbf{K}$ is the permeability or hydraulic conductivity of the porous medium and the velocity $\mathbf{u}$ of the phase is given by the Darcy law as $\mathbf{u} = -\mathbf{K}\,\mathrm{grad}\,p$.

The rest of the paper is organised as follows. Section 2 presents two-point finite volume discretization on adaptive and uniform meshes. Section 3 presents adaptivity criterion and an adaptive algorithm. In the Section 4, an extensive numerical analysis of singular problems on adaptive and uniform meshes is reported and finally Section 5 concludes the paper.

2. Two-point finite volume discretization

For solving partial differential equations (PDEs) in a domain, by numerical methods such as the 2P-FVM, the domain is divided into smaller elements (meshing of the domain) called finite volumes or cells. Integrating equation (1) over one of the finite volumes V in the mesh and using the Gauss divergence theorem leads to:

$$-\int_{\partial V} \mathbf{K}\nabla p \cdot \hat{\mathbf{n}} \; \mathrm{d}\sigma = \int_V f \mathrm{d}\tau, \tag{3}$$

where $\hat{\mathbf{n}}$ is the unit outward normal on the boundary ∂V of the finite volume V. Let us assume that finite volumes V are rectangular, and the boundary of these finite volumes consists of four segments ∂V_i. Thus, the above equation can be written as:

$$-\sum_{i=1}^{4} \int_{\partial V_i} \mathbf{K}\nabla p \cdot \hat{\mathbf{n}} = \int_V f. \tag{4}$$

The term $-\int_{\partial V_i} \mathbf{K}\nabla p \cdot \hat{\mathbf{n}}$ is referred to as the flux through the edge ∂V_i. Let us denote it by $\mathscr{F}_i$. Hence, equation (4) can be written as:

$$\sum_{i=1}^{4} \mathscr{F}_i = \int_V f. \tag{5}$$

The degrees of freedom (DOF) for the 2P-FVM (Aavatsmark, 2002; Eigestad and Klausen, 2005) lie at the cell centers. Each finite volume in the mesh gives rise to a discrete equation (5). Collecting all such equations results in a discrete system $\mathbf{A}\mathbf{p}_h = \mathbf{b}$.

Now, let us compute the flux for the interface MN shared by the cells 1 and 2 (Figure 1(a)). Two-point approximation of the flux (Aavatsmark, 2002; Ewing *et al.*, 1991a, b) through the edge MN is given as:

$$F_{\mathrm{MN}} = \Phi_{\mathrm{MN}}(p_2 - p_1), \tag{6}$$

where the scalar Φ_{MN} is referred to as the transmissibility of the interface MN and is given as:

$$\Phi_{\mathrm{MN}} = K_1 K_2 \left(\frac{l}{h_1 h_2}\right) \frac{1}{(K_1/h_1 + K_2/h_2)}. \tag{7}$$

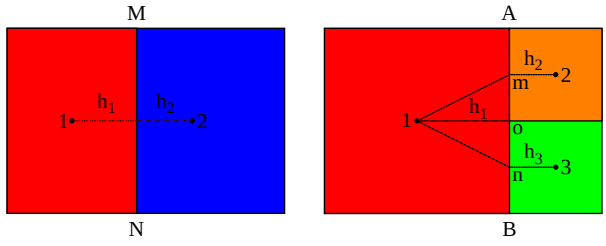

Flux on a matching grid. (a)

Flux on a non-matching grid. (b)

Figure 1.
Computation of flux across an edge

Here, K_1 and K_2 refers to the permeability of the cells 1 and 2 in Figure 1(a). The perpendicular distance of the interface MN from the center of cell 1 is h_1. Similarly, h_2 is the perpendicular distance of the interface MN from the center of cell 2. The length of interface MN is l.

Adaptive discretization can result in a non-matching grid as shown in Figure 1(b). We are using the TPFA for computing flux on a non matching grid. The flux through the interfaces AO and BO on the non-matching grid (Figure 1(b)) is given as follows:

$$\mathscr{F}_{\mathrm{AO}} = \Phi_{\mathrm{AO}}(p_2 - p_1), \tag{8}$$

$$\mathscr{F}_{\mathrm{BO}} = \Phi_{\mathrm{BO}}(p_3 - p_1), \tag{9}$$

where p_1, p_2 and p_3 are the pressures of cells 1-3, respectively. The transmissibilities Φ_{AO} and Φ_{BO} of the interfaces AO and BO are given as:

$$\Phi_{\mathrm{AO}} = K_1 K_2 \left(\frac{l_1}{h_1 h_2}\right) \frac{1}{(K_1/h_1 + K_2/h_2)}, \tag{10}$$

$$\Phi_{\mathrm{BO}} = K_1 K_3 \left(\frac{l_2}{h_1 h_3}\right) \frac{1}{(K_1/h_1 + K_3/h_3)}. \tag{11}$$

Here, l_1 is the length of interface AO and l_2 is the length of interface OB. F_{AO} and F_{BO} are the fluxes through edges AO and BO, respectively. K_1-K_3 refers to the permeabilities of cells 1-3 (Figure 1(b)). The total flux through edge AB is given as the sum of the fluxes through the edges OA and OB. That is $\mathscr{F}_{\mathrm{AB}} = \mathscr{F}_{\mathrm{OA}} + \mathscr{F}_{\mathrm{OB}}$.

The author wants to point out that the 2P-FVM flow equations (8) and (9) based on Figure 1(b) are prone to accuracy problems when modeling multiphase flow with natural heterogeneities and near sharp fluid phase fronts (sharp saturations differences). For these cases, the simple 2P-FVM approximation is not enough, and the flux calculation should also consider at least two more neighbouring cells (Garcia and Pruess, 2000; Hermitte and Guerillot, 1993; Pruess and Garcia, 2000).

3. Adaptive criteria and adaptive algorithm

The presented criterion has been extensively used in the finite element community (Morin *et al.*, 2000; Verfürth, 1994; Chen and Dai, 2002). Let a mesh consist of N finite volumes/cells Ω_i, $i = 1, 2, \ldots N$ and let p_h be the finite volume solution on this mesh. Let p be the exact solution. From equation (1), the residual r can be defined as:

$$r = f - \nabla \cdot (-\mathbf{K}\nabla p_h). \tag{12}$$

Integrating and using the Gauss divergence theorem results in:

$$\int_\Omega r \, \mathrm{d}\tau = \int_\Omega f \, \mathrm{d}\tau + \int_{\partial\Omega} (\mathbf{K}\nabla p_h) \cdot \hat{\mathbf{n}} \, \mathrm{d}\sigma, \tag{13}$$

and taking the modulus of both sides and applying the triangle inequality to the right hand side:

$$\left| \int_\Omega r \, \mathrm{d}\tau \right| \leq \left| \int_\Omega f \, \mathrm{d}\tau \right| + \left| \int_{\partial\Omega} (\mathbf{K}\nabla p_h) \cdot \hat{\mathbf{n}} \, \mathrm{d}\sigma \right|, \tag{14}$$

$$\left|\int_{\Omega} r\,\mathrm{d}\tau\right| \leq \left|\sum_{i=1}^{N}\int_{\Omega_i} f\,\mathrm{d}\tau\right| + \left|\sum_{i=1}^{N}\int_{\partial\Omega_i}(\mathbf{K}\nabla p_h)\cdot\hat{\mathbf{n}}\,\mathrm{d}\sigma\right|, \tag{15}$$

where N is the total number of finite volumes/cells in the mesh:

$$\left|\int_{\Omega} r\,\mathrm{d}\tau\right| \leq \sum_{i=1}^{N}\left|\int_{\Omega_i} f\,\mathrm{d}\tau\right| + \sum_{i=1}^{N}\left|\int_{\partial\Omega_i}(\mathbf{K}\nabla p_h)\cdot\hat{\mathbf{n}}\,\mathrm{d}\sigma\right|. \tag{16}$$

Using the Cauchy-Schwarz inequality. That is $|\int f| \leq \|f\|_{L_2}\|1\|_{L_2}$:

$$\left|\int_{\Omega} r\,\mathrm{d}\tau\right| \leq \sum_{i=1}^{N}\left[\|f\|_{L^2(\Omega_i)}|\Omega_i|^{1/2}\right] + \sum_{i=1}^{N}\left[\|\mathbf{K}\nabla p_h)\cdot\hat{\mathbf{n}}\|_{L^2(\partial\Omega_i)}|\partial\Omega_i|^{1/2}\right], \tag{17}$$

$$\left|\int_{\Omega} r\,\mathrm{d}x\right| \leq \sum_{i=1}^{N}\left[\|f\|_{L^2(\Omega_i)}|\Omega_i|^{1/2} + \|(\mathbf{K}\nabla p_h)\cdot\hat{\mathbf{n}}\|_{L^2(\partial\Omega_i)}|\partial\Omega_i|^{1/2}\right], \tag{18}$$

$$\left|\int_{\Omega} r\mathrm{d}x\right| \leq \sum_{i=1}^{N} r_i. \tag{19}$$

We are using the following expression for computing the error from the cell i in a mesh:

$$\varepsilon_i \stackrel{\text{def}}{=} \left[\|f\|_{L^2(\Omega_i)}|\Omega_i|^{1/2} + \|(\mathbf{K}\nabla p_h)\cdot\hat{\mathbf{n}}\|_{L^2(\partial\Omega_i)}|\partial\Omega_i|^{1/2}\right]. \tag{20}$$

Here, $|\Omega_i|$ is the area of the finite volume, $|\partial\Omega_i|$ is the circumference of the finite volume, and $\hat{\mathbf{n}}$ is the unit outward normal. The quantity $\|(\mathbf{K}\nabla p_h)\hat{\mathbf{n}}\|_{L^2(\partial\Omega_i)}|\partial\Omega_i|^{1/2}$ is the total flux associated with cell i. Let us further define a quantity named adaptivity index for cell i in a mesh:

$$\eta_i \stackrel{\text{def}}{=} \left[\frac{\varepsilon_i}{\max\limits_{j\in\text{cells}}\varepsilon_j}\right]. \tag{21}$$

It can be seen from the above definition of adaptivity index. For a cell with zero error ($\varepsilon = 0$), the adaptivity index η is zero, and for a cell with maximum error η is 1. Thus, for any cell, the adaptivity index η_i will be in the range [0,1]. It can be seen in the Algorithm 1 that the driving force for the algorithm is the adaptivity index η.

The adaptivity index (equation (21)) drives the Algorithm 1 by selecting some finite volumes for further refinement. Apart from the driving force, another important aspect of an algorithm is its stopping criteria. We are using three stopping criteria. The first two criteria are quite obvious. Our first criterion "DOF $\leq$ $\text{DOF}_{\max}$" is the maximum allowable $\text{DOF}_{\max}$ or the maximum allowed mesh refinement. The second criterion "Iter $\leq$ $\text{Iter}_{\max}$" is the maximum allowed adaptive iteration steps (Figure 2).

The third criterion "$\xi_k/\xi_0 \leq$ tol" is the error reduction after k iteration steps of the adaptive algorithm. Here, ξ_k denotes the maximum error (maximum value of ε_i on a mesh) on an adaptively refined mesh after k iteration steps of the adaptive Algorithm 1 (Figure 3). ξ_0 is the maximum error on the initial mesh. The quantity ξ_k/ξ_0, which

measures the reduction of the a posteriori error estimate, provides some information of the relative error reduction. Thus, ξ_k/ξ_0 can be used as a stopping criterion apart from the maximum number of DOF.

Algorithm 1 is used for adaptive refinement. When a finite volume is selected for further refinement based on the value of the adaptivity index (equation (21)), this finite volume is divided into four equal finite volumes as shown in Figure 2. During the adaptive refinement process, all finite volumes Ω_i in a mesh, for which the adaptivity index η_i is greater than a given tolerance δ, are refined. The tolerance δ lies between the values 0 and 1. Tolerance δ equal to 0 means uniform refinement (refine all finite volumes), and tolerance δ equal to 1 means that the adaptive algorithm will refine a single finite volume per iteration step which can be costly. Both of these values can be computationally expensive and may not be optimal. A small δ will refine many finite volumes and thus introduce many new cells per iteration step of the adaptive algorithm. On the other hand, a large value of δ will refine fewer cells and thus introduce fewer new finite volumes per iteration step. It should be kept in mind that during each iteration step of the adaptive algorithm a discrete system needs to be solved. Typically a value of $\delta = 0.5$ is used (Riviere, 2000).

To measure the effectiveness of the adaptivity index (equation (21)) in selecting the cells with maximum error, we use the relation:

$$\Gamma \stackrel{\text{def}}{=} \frac{\text{Cell number with } \eta = 1.0}{\text{Cell number with maximum point-wise error } |p - p_h|}. \tag{22}$$

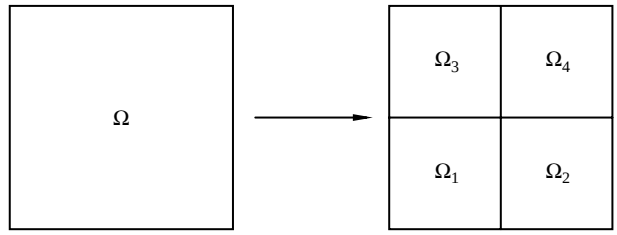

Figure 2.
Refinement of the cell Ω into four cells Ω_i, $i = 1, \ldots, 4$

Algorithm1: Adaptive Algorithm.

```
Mesh the domain;
Set Iteration Counter k = 0;
while DOF ≤ DOF_max or Iter ≤ Iter_max or [ξ_k = ξ_0] ≥ tol do
    Discretize the PDE on the mesh by the 2P-FVM;
    Solve the discrete system to a given tolerance;
    forall (FiniteVolumes j in the Mesh) do
        if (η_j ≥ δ) then
            Refine the Finite Volume j;
        end
    end
    Form a new mesh;
    k++;
end
```

Figure 3.

Here, Γ is the robustness of the indicator η. If Γ is close to 1, the cells with the maximum point-wise error and the cells with the maximum error given by the error indicator (equation (20)) are the same. We compute the robustness quantity Γ of the adaptive index during each iteration step of the adaptive Algorithm 1.

4. Numerical examples

Let us mention norms for measuring convergence rate. Let $\mathbf{p}$ be the exact solution vector and $\mathbf{p}_h$ be the finite volume solution vector on a mesh. Let us further assume that p^k be the exact pressure at the center of the cell k and p_h^k be the discrete pressure by the finite volume approximation for the same location. Error in the L_∞ norm is defined as:

$$\|\mathbf{p} - \mathbf{p}_h\|_{L_\infty} \stackrel{\text{def}}{=} \max_{k \in \text{cells}} \left[|p^k(x) - p_h^k(x)| \right] \tag{23}$$

Error in the L_2 norm is defined as:

$$\|\mathbf{p} - \mathbf{p}_h\|_{L_2} \stackrel{\text{def}}{=} \left(\sum_{\text{cells}} \left[p^k(x) - p_h^k(x) \right]^2 \ \Omega_k \right)^{1/2}. \tag{24}$$

Here, Ω_k is the area/volume of the finite volume k in the mesh. Let $\mathbf{u}$ be the exact Darcy velocity through the center of an edge $\mathscr{E}$, and $\mathbf{u}_h$ be the discrete Darcy velocity by the finite volume method through the center of the same edge $\mathscr{E}$. Further, let $\hat{\mathbf{n}}$ be the normal to the edge $\mathscr{E}$ and the magnitude of normal vector $\hat{\mathbf{n}}$ is equal to the length of the edge $\mathscr{E}$. The velocity error on a mesh in the $L_2(\Omega)$ norm is defined as:

$$\|\mathbf{u} - \mathbf{u}_h\|_{L_2} \stackrel{\text{def}}{=} \left(\sum_{\text{cells}} \sum_{\text{edges}} \left[|(\mathbf{u} - \mathbf{u_h}) \cdot \hat{\mathbf{n}}| \right]^2 \right)^{1/2}. \tag{25}$$

For a mesh, we measure errors in the norms given by the equations (23)-(25). We have implemented the presented computational approach in the C++ language. The software package is freely available at the web page www.mi.uib.no/ $\sim$ sanjay

For all numerical experiments, the exact solution is given by an analytical form. The finite volume solution is enforced inside the domain by the Dirichlet boundary condition and the source term. For solving the discrete systems of equations formed on the sequence of adaptive and uniform meshes, we are using the ILU preconditioned CG iterative solver unless mentioned otherwise. Let the domain be $\Omega = [-1, 1] \times [-1, 1]$, and it is divided into four sub-domains according to the permeability K (Figure 4). Let the permeability in the sub-domain Ω_i be K_i. It is assumed that the permeability in the sub-domain Ω_1 is equal to the permeability in the sub-domain Ω_3, and the permeability in the sub-domain Ω_2 is equal to the permeability in the sub-domain Ω_4. That is $K_1 = K_3$ and $K_2 = K_4$. Let us further assume that $K_1 = K_3 = R$ and $K_2 = K_4 = 1$. The parameter R is defined below. Let the exact solution in polar form be (Chen and Dai, 2002; Morin *et al.*, 2000):

$$p(r, \theta) = r^\gamma \eta(\theta). \tag{26}$$

The parameter γ denotes the singularity in the solution (Chen and Dai, 2002) and it depends on the permeability distribution in the domain (see Figure 5(a) and 5(b) for the permeability distribution for the singularities $\gamma = 0.1$ and $\gamma \approx 0.13$). $\eta(\theta)$ is given as:

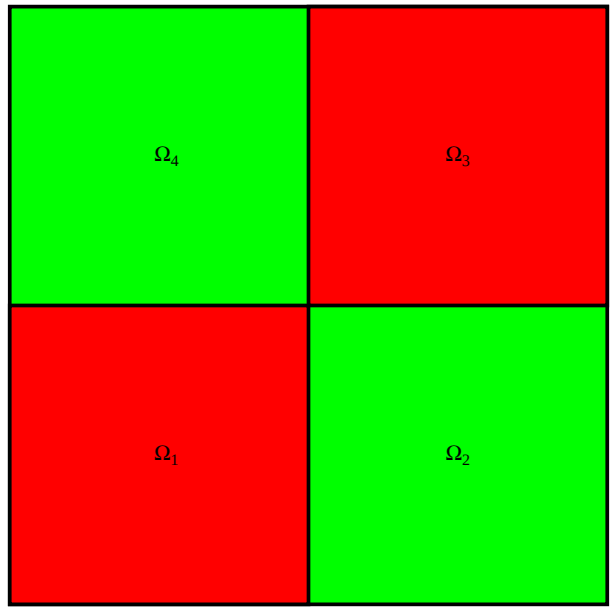

Figure 4.
Domain Ω is divided into four sub-domains Ω_i, $i = 1, \ldots, 4$ according to the permeability

Notes: Permeability in the sub-domain Ω_i is K_i.We are assuming $K_1 = K_3 = R$ and $K_2 = K_4 = 1$

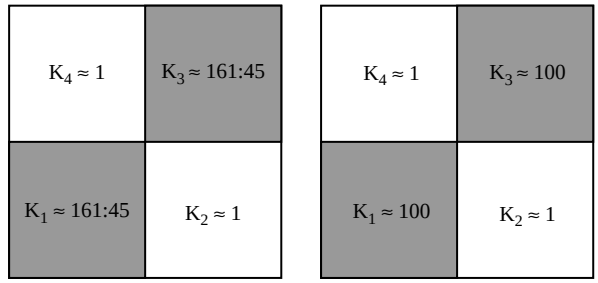

$\gamma = 0.1$. $\gamma = 0.126902$.

(a) **(b)**

Figure 5.
Permeability distribution for the singularities $\gamma = 0.1$ and $\gamma = 0.1269$

Note: The solution is singular at $O = (0,0)$

$$\eta(\theta) = \begin{cases} \cos[(\pi/2 - \sigma)\gamma]\ \cos[(\theta - \pi/2 + \rho)\gamma], & \theta \in [0, \pi/2], \\ \cos(\rho\gamma)\ \cos[(\theta - \pi + \sigma)\gamma], & \theta \in [\pi/2, \pi], \\ \cos(\sigma\gamma)\ \cos[(\theta - \pi - \rho)\gamma], & \theta \in [\pi, 3\pi/2], \\ \cos[(\pi/2 - \rho)\gamma]\ \cos[(\theta - 3\pi/2 - \sigma)\gamma], & \theta \in [3\pi/2, 2\pi], \end{cases} \tag{27}$$

and the parameters R, γ, ρ and σ satisfy the following nonlinear equations:

$$\begin{cases} R = -\tan[(\pi - \sigma)\gamma]\ \cot(\rho\gamma), \\ 1/R = -\tan(\rho\gamma)\ \cot(\sigma\gamma), \\ R = -\tan(\sigma\gamma)\ \cot[(\pi/2 - \rho)\gamma], \end{cases} \tag{28}$$

under the following nonlinear constraints:

$$\begin{gathered} 0 < \gamma < 2, \\ \max\{0, \pi\gamma - \pi\} < 2\gamma\rho < \min\{\pi\gamma, \pi\}, \\ \max\{0, \pi - \pi\gamma\} < -2\gamma\rho < \min\{\pi, 2\pi - \pi\gamma\}. \end{gathered} \tag{29}$$

The constrained nonlinear equation (28) can be solved for the parameters R, σ, and ρ by Newton's iteration algorithm for different degrees of singularity γ. The analytical solution $p(r,\theta)$ satisfies the usual interface conditions p and $\mathbf{K}(\partial p/\partial \mathbf{n})$ are continuous across the interfaces. It can be shown that the solution p belongs in the fractional Sobolev space $\mathbf{H}^{1+\kappa}(\Omega)(\kappa < \gamma)$ (Strang and Fix, 1973).

4.1 Capturing singularity by adaptive and uniform refinements

Let the singularity be $\gamma = 0.1$. Various parameters that satisfy the relation (28) under the constraint (29) are:

$$R \approx 161.4476, \quad \rho \approx 0.7854 \text{ and } \sigma \approx -14.9225.$$

The permeability distribution is shown in Figure 5(a). The exact solution belongs to the fractional Sobolev space $\mathbf{H}^{1+k}(k < 0.1)$. We have solved this problem on adaptive and uniform meshes. The outcome of our numerical work is shown in Figures 6-8. Figure 6(a) is a surface plot of the exact solution. The solution is singular at the origin. Figure 6(b) shows a surface plot of the error. It can be seen that the error is maximum at the singularity. Figure 7 compares the convergence behaviour on adaptive and uniform meshes in the L_∞ norm. We did not notice any convergence in the L_∞ norm on uniform meshes till 1 million DOF. A similar behaviour was also observed in Eigestad and Klausen (2005) on uniform

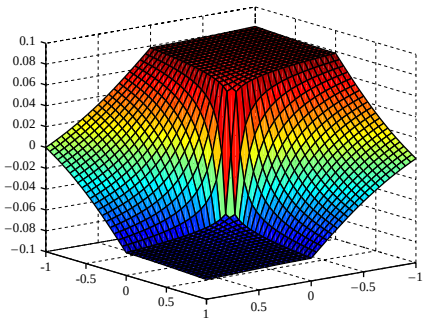

Exact solution given by the equation (26) for $\gamma = 0{:}1$.

(a)

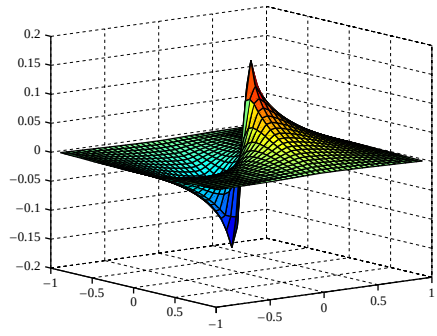

Surface plot of the error $(u - uh)/||u||_{L\infty}$ for $\gamma = 0{:}1$.

(b)

Figure 6.
Surface plots of the exact solution and error for the singularity parameter $\gamma = 0.1$

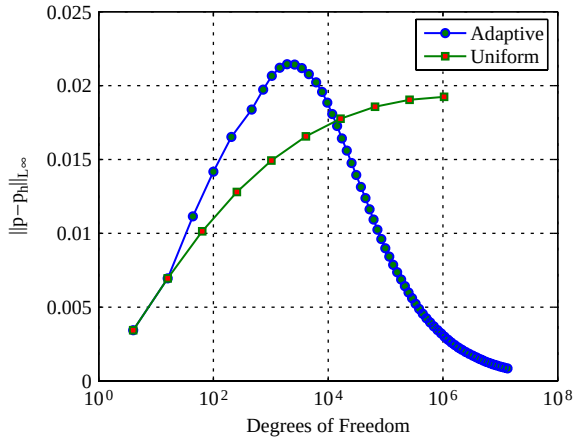

Figure 7.
On adaptive meshes
$\|\mathbf{p} - \mathbf{p}_h\|_{L_\infty} \approx \mathrm{DOF}^{-1.0/2}$

Notes: On uniform meshes, there is no convergence till 1 million DOF. The solution is in H^{1+k} ($k < 0.1$)

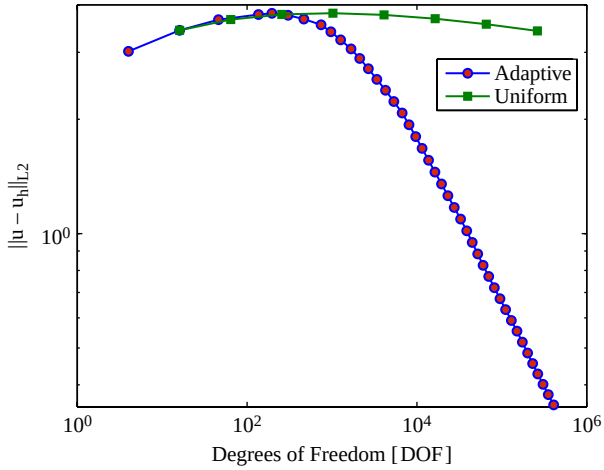

Figure 8.
On adaptive meshes
$\|\mathbf{u} - \mathbf{u}_h\|_{L_\infty} \approx \mathrm{DOF}^{-1.0/2}$

Notes: On uniform meshes, there is no convergence till 1 million DOF. The solution is in H^{1+k} ($k < 0.1$)

meshes for singular problems. It was suggested in Eigestad and Klausen (2005) that adaptive meshes may be ideal for such solutions. On adaptive meshes, we are getting $\|\mathbf{p} - \mathbf{p}_h\|_{L_\infty} \approx \mathrm{DOF}^{-p/2}$ with the convergence $P \approx 1$ (Figure 7). Because of the regularity of the solution, this convergence is quasi optimal (Chen and Dai, 2002; Morin *et al.*, 2000). Convergence of the Darcy flux on adaptive and uniform meshes is shown in Figure 8. On uniform meshes, the convergence of the Darcy flux is approximately equal to the regularity of the solution. On the other hand, the method is converging with a rate approximately equal to 1 on the adaptive meshes.

Let the singularity be $\gamma = 0.1269$. Various parameters that satisfy the relation (28) under the constraint (29) are:

$$R \approx 99.999999, \quad \rho \approx 0.7853982 \text{ and } \sigma \approx -11.59263.$$

The permeability distribution in the domain is shown in Figure 5(b). The exact solution belongs in the fractional Sobolev space $\mathbf{H}^{1.126}$. Figure 9 is comparing the convergence behaviour of the 2P-FVM on adaptive and uniform meshes. Again, we did not observe any convergence till 1 million DOF on uniform meshes (there is some convergence during the last refinement (Figure 9)). While on the adaptive meshes, we are still getting $\|\mathbf{p} - \mathbf{p}_h\|_{L_\infty} \approx \text{DOF}^{-P/2}$ with $P \approx 1.0$.

Figure 10 is a plot of the third stopping parameter ξ_k/ξ_0 (see the Algorithm 1) against the DOF in the sequence of generated meshes. Here, k is the iteration counter in the algorithm. Solutions are in the spaces $\mathbf{H}^{1.13}$ and $\mathbf{H}^{1.1}$. It is clear that the stopping parameter decreases with adaptive mesh refinement as was claimed in the Section 3.

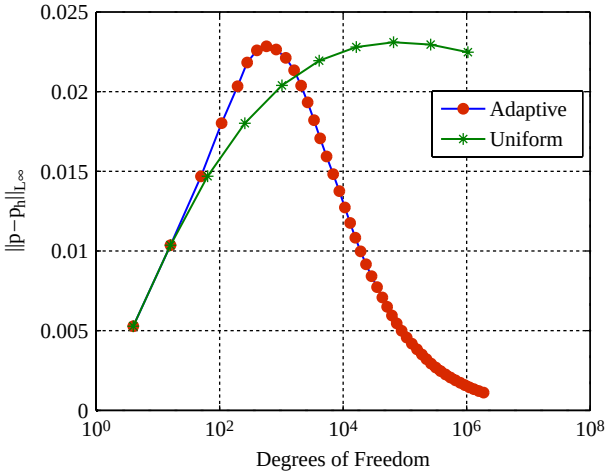

Figure 9.
On adaptive meshes $\|\mathbf{p} - \mathbf{p_h}\|_{L_\infty} \approx \text{DOF}^{-1.0/2}$

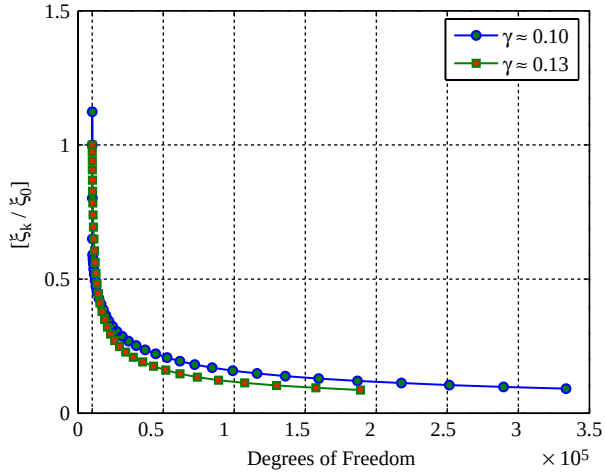

Figure 10.
Decrease in the stopping criteria ξ_k/ξ_0 in the Algorithm 1 with adaptive refinement

So, it can be used as a stopping criterion. It is a more robust stopping criterion than the number of DOF because the DOF does not tell us how much error has reduced.

4.2 Robustness of the adaptivity index η

Figure 11 is a plot of the robustness against the iterations of the adaptive algorithm. It can be seen in the Figure 11, the robustness is almost always equal to 1.0 for all of the adaptive iterations. It means that the cells with the maximum point-wise error and cells

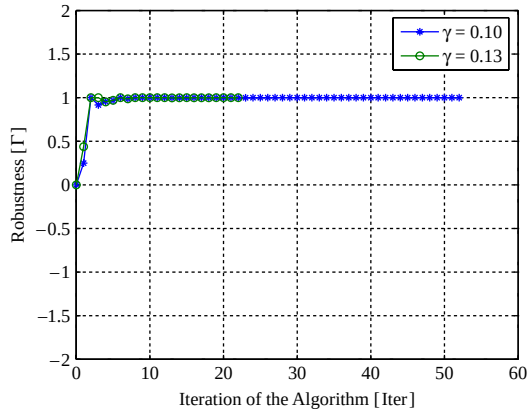

Note: Solutions are in the spaces $H^{1.126902}$ and $H^{1.1}$

Figure 11.
Robustness (defined by the equation (22)) of the adaptivity index for finding cells with most error

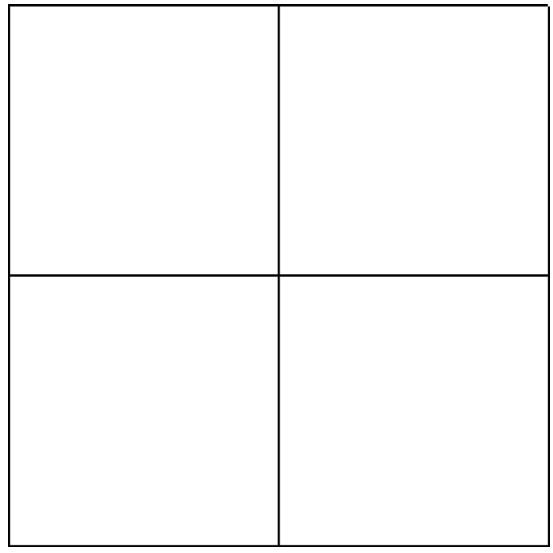

Notes: Meshes are very dense at the location (origin) of the singularity and also in the region of high permeability. See the permeability distribution in the Figure5(a). The singularity parameter $\gamma = 0.1$

Figure 12.
Adaptive meshes generated by the algorithm, area of the smallest cell $= 1.0$

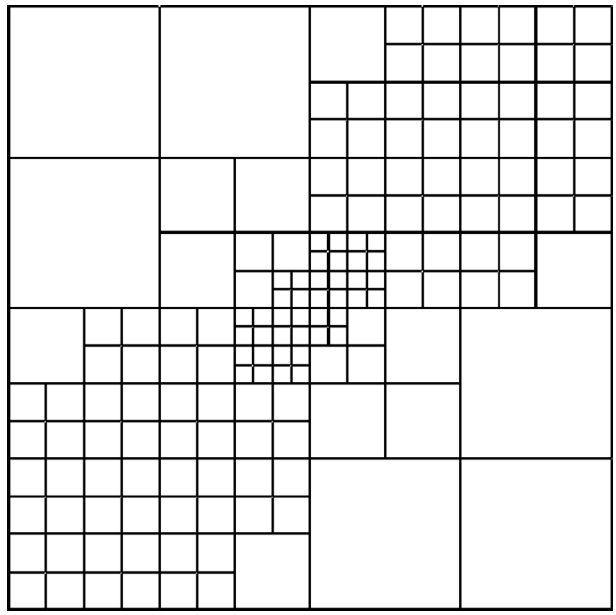

Note: See note to Figure 12

Figure 13.
Adaptive meshes generated by the algorithm, area of the smallest cell $\approx 3.91 \times 10^{-3}$

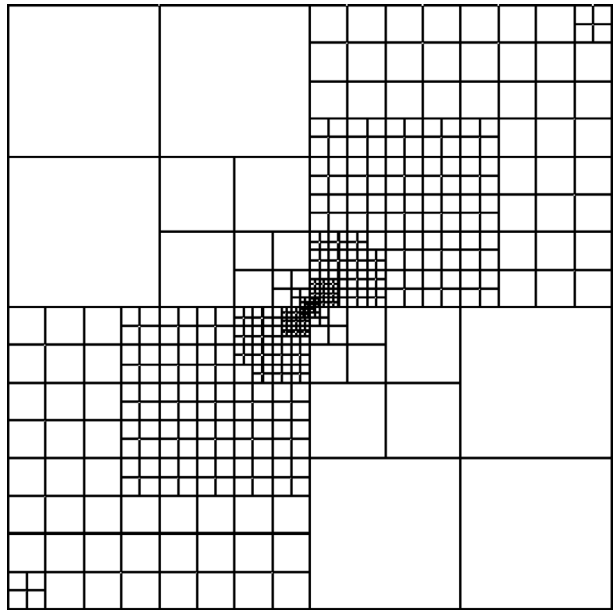

Note: See note to Figure 12

Figure 14.
Adaptive meshes generated by the algorithm, area of the smallest cell $\approx 6.10 \times 10^{-5}$

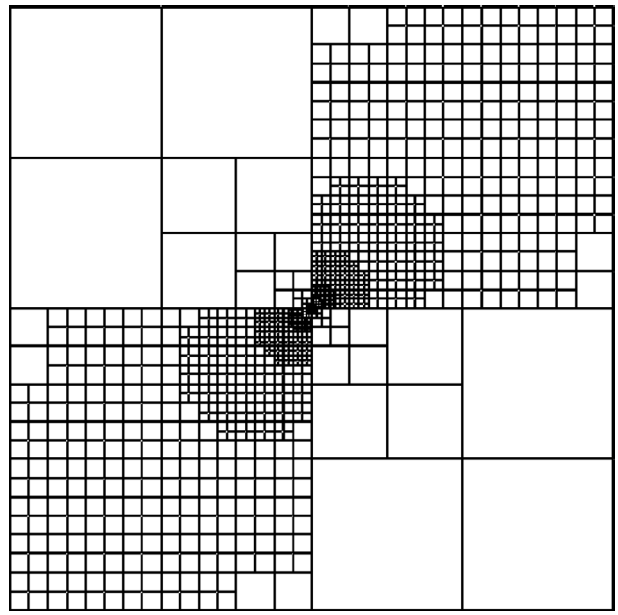

Note: See note to Figure 12

Figure 15.
Adaptive meshes generated by the algorithm, area of the smallest cell $\approx 9.54 \times 10^{-7}$

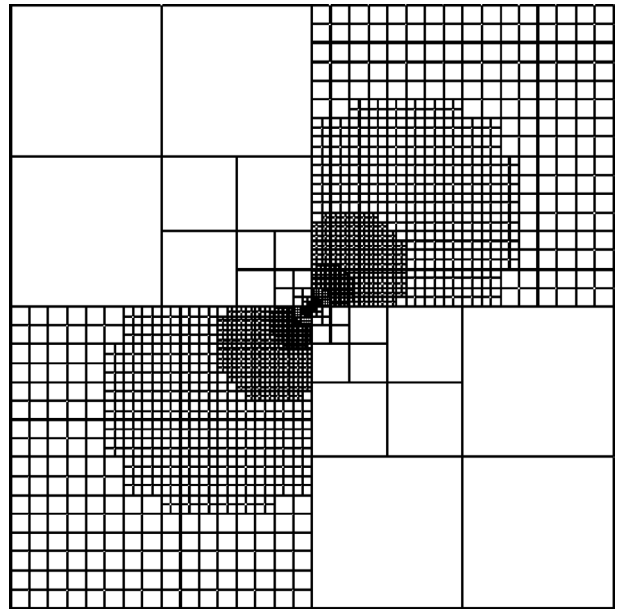

Note: See note to Figure 12

Figure 16.
Adaptive meshes generated by the algorithm, area of the smallest cell $\approx 3.73 \times 10^{-9}$

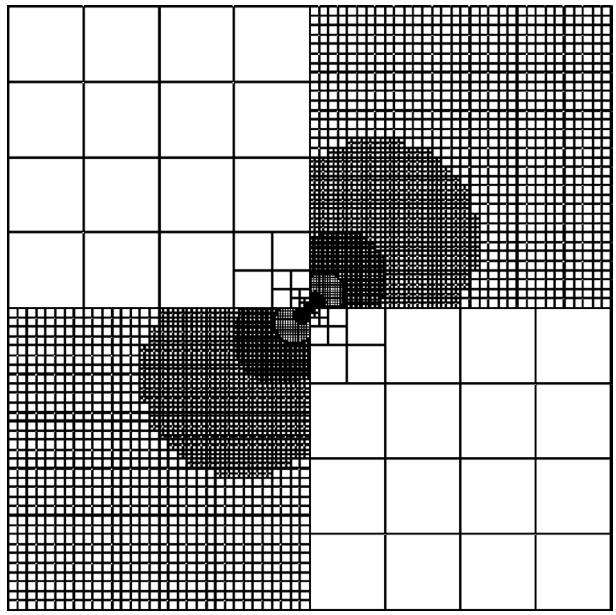

Note: See note to Figure 12

Figure 17.
Adaptive meshes generated by the algorithm, area of the smallest cell $\approx 9.09 \times 10^{-13}$

with the maximum value of the error indicator given by the equation (20) are the same. Figures 12-17 show adaptively generated meshes for the singularity $\gamma = 0.1$. See Figure 4(a) for permeability distribution in the domain. Dense meshes are expected at the origin due to singular nature of the solution. It can be seen in the figures that the adaptive algorithm together with the adaptivity criterion are creating DOF at the right place. It is interesting to notice that the meshes are also dense in the higher permeability sub-domains (sub-domains 1 and 3) compared to the meshes in the sub-domains with lower permeability (sub-domains 2 and 4). It can be explained on the basis of high flux in these sub-domains. The adaptive algorithm is trying to equi-distribute the error indicator (equation (20)) over all cells in the mesh. One term in the error indicator ε given by the equation (20) is flux, and the flux ($\mathbf{K}\nabla p$) is high in the sub-domains with higher permeability.

4.3 Convergence in the L_2

Figure 18 shows convergence behaviour of pressure in the L_2 norm on adaptive meshes. On adaptive meshes, pressure in the L_2 norm is converging as:

$$\|\mathbf{p} - \mathbf{p}_h\|_{L_2} \approx \mathrm{DOF}^{-2/2}.$$

Thus, the L_2 convergence rate of pressure is approximately 2.0. The convergence is independent of the solution regularity.

4.4 Convergence in the L_∞

Figure 19 shows the convergence behaviour of pressure in the L_∞ norm on adaptive meshes. On adaptive meshes pressure is converging as:

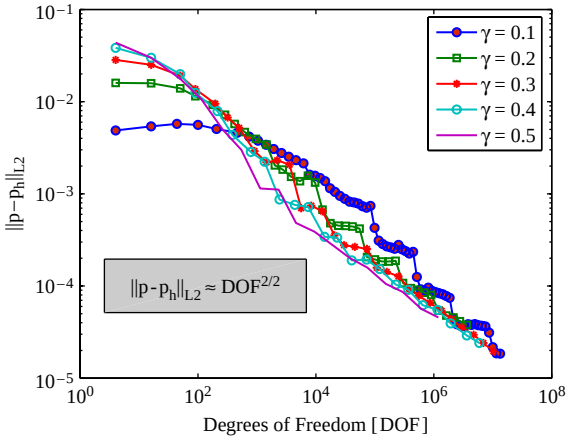

Figure 18.
L_2 convergence of pressure on adaptive meshes

Note: Pressure converges as $\|p - p_h\|_{L_2} \approx DOF^{-2/2}$

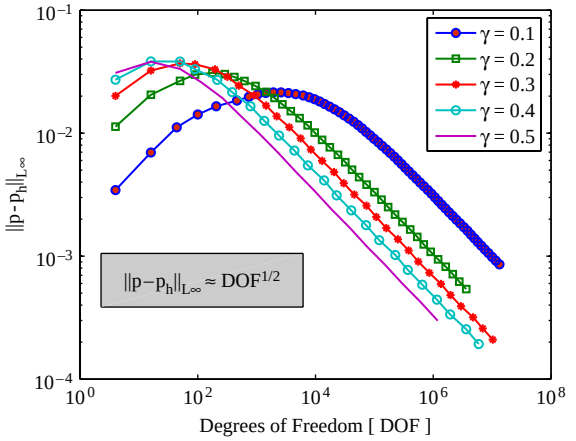

Figure 19.
Point wise convergence of pressure on adaptive meshes

Note: Pressure converges as $\|p - p_h\|_{L_\infty} \approx DOF^{-1/2}$

$$\|\mathbf{p} - \mathbf{p}_h\|_{L_\infty} \approx \mathrm{DOF}^{-1/2}.$$

Thus, the point-wise convergence rate of pressure is approximately 1.0. The convergence does not depend on the singular nature of the solution.

4.5 Flux convergence

Figure 20 shows the convergence behaviour of the Darcy velocity on adaptive meshes. On adaptive meshes Darcy velocity is converging as:

$$\|\mathbf{u} - \mathbf{u}_h\|_{L_2} \approx \mathrm{DOF}^{-0.95/2}.$$

Thus, the convergence rate of the Darcy velocity is approximately 1.0 and it does not depend on the singular nature of the solution.

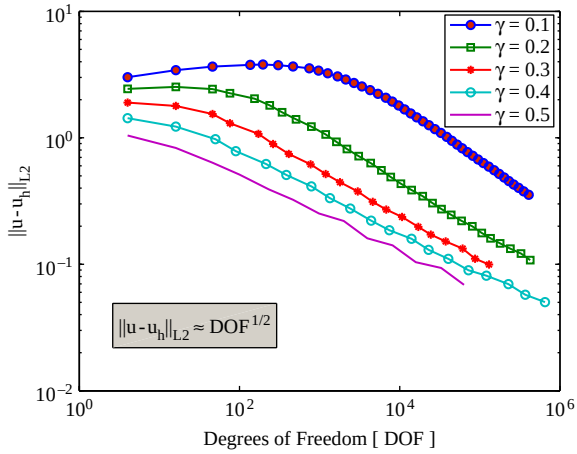

Note: Darcy flux converges as $\|u - u_h\|_{L_2} \approx \text{DOF}^{-1/2}$

Figure 20.
Convergence of Darcy flux on adaptive meshes

4.6 The δ effect

The adaptive Algorithm 1 depends on many parameters such as the adaptivity index η and the parameter δ. Most of these parameters also depend on each other. Thus, finding an optimal mesh is a nonlinear problem. The parameter δ is an important ingredient of the Algorithm 1. Based on the value of δ, the algorithm refines the finite volumes. A higher value of δ means that the algorithm will refine fewer cells, while for a lower value of δ, the algorithm will refine many cells. For example, if $\delta = 0$, the algorithm will refine all the cells in the mesh, and if $\delta = 1$, the algorithm will refine only one cell. Both of these situations can be costly. For the singularity parameter $\gamma = 0.1$, we run the algorithm for three values of δ (0.5, 0.6, 0.7). Figure 21 shows the outcome of our work. It can be seen in Figure 21 that for a given DOF, $\delta = 0.5$ is a better choice. It should be

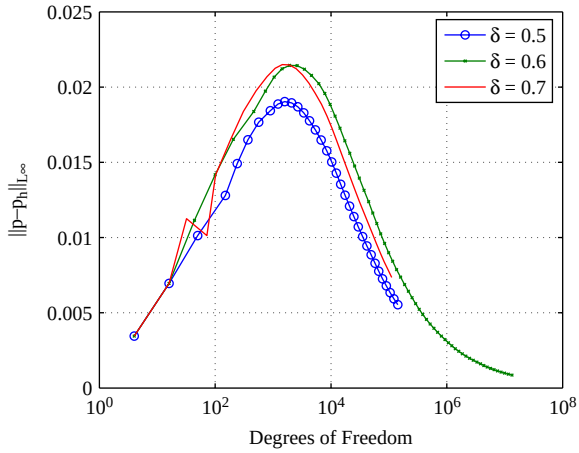

Note: See the Algorithm 1 for δ

Figure 21.
Effect of δ

noted that the number of iteration steps of the adaptive algorithm increases with increasing value of δ. Thus, the computational work required for $\delta = 0.5$ is lower than the work required for $\delta = 0.6$ and $\delta = 0.7$. Of these three values of δ, $\delta = 0.5$ is optimal. It requires the least amount of computational work for a given tolerance.

4.7 Singularity and size of finite volumes

In this example, we explore how the degree of singularity and density of mesh (area of the smallest cell) are related. For a highly dense mesh, the area of the smallest finite volume or cell is very small. It is expected that as the degree of singularity increases or the parameter γ decreases, the adaptive algorithm will create denser and denser meshes or meshes with smaller and smaller cells. Figure 22 shows the area of the smallest cell in a mesh versus the DOF of the mesh for various degree of singularity parameter ($\gamma = 0.1, 0.2, 0.3$). It can be seen in this figure, for a given DOF the density of the mesh or the area of the smallest element depends on the regularity of the solution.

4.8 Which are better conditioned meshes – uniform or adaptive?

The 2P-FVM on both adaptive and uniform meshes produces symmetric and positive definite system (SPD). We use the CG for solving the SPD systems. In this example, we compare the condition number of the discrete systems associated with the uniform and adaptive meshes. We see that adaptive meshes produce better conditioned systems than formed on the uniform meshes for a given DOF. Tolerance for solving the systems by CG is 1.0×10^{-10}.

For the singularity $\gamma = 0.1$, Figure 23 compares the number of CG-iterations (without any preconditioner) required for solving systems associated with adaptive and uniform meshes. It can be seen in this figure that for a given DOF the number of iterations required for solving a discrete system associated with a uniform mesh is approximately three times the number of iterations required for solving a discrete system associated with an adaptive mesh. Thus, from theory (Vorst, 2003, Chapter 5), it

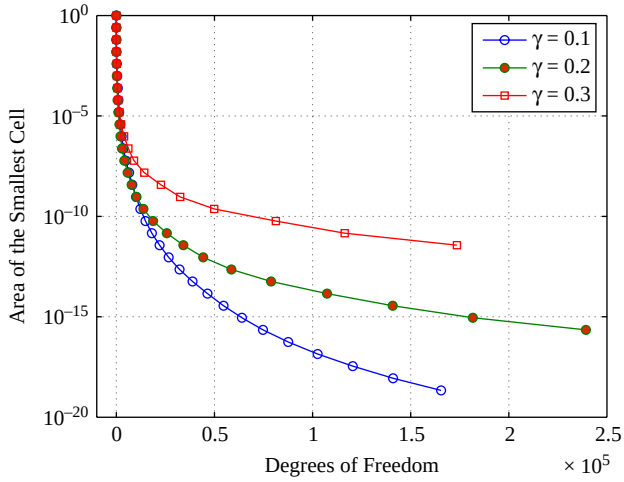

Figure 22.
Area of the smallest cell in an adaptive mesh vs the number of cells

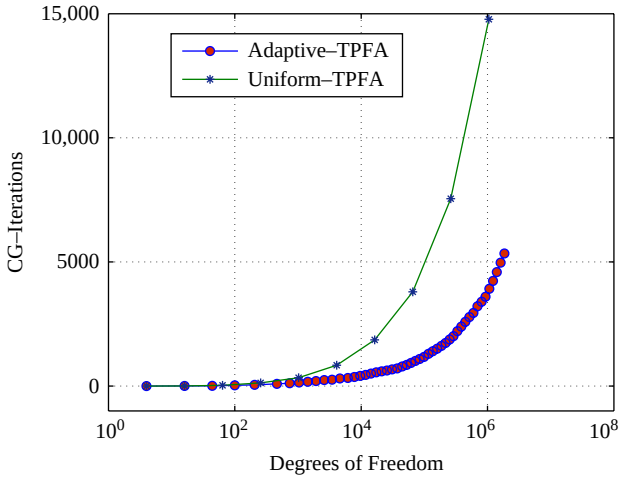

Figure 23.
Number of CG-iterations (without any preconditioner) versus DOF for uniform and adaptive meshes $\gamma = 0.1$

is clear that the condition number of a discrete system associated with the uniform mesh is approximately nine times the condition number of a discrete system formed on an adaptive mesh. Adaptive algorithm generates not only more accurate discrete systems but also better conditioned one compared to discrete systems associated with uniform meshes.

5. Conclusions

We have formulated and analysed the 2P-FVM on adaptive meshes. An adaptive criterion and an adaptive algorithm is also presented. Extensive numerical work of practical importance is reported for validating the presented computational technique. Similar concepts can be directly extended to 3D problems. We would like to conclude the paper by the following three points:

(1) Compared to other expensive discretization techniques, 2P-FVM discretization on adaptive and uniform meshes results in a symmetric SPD. There are various well developed and efficient solvers for SPD systems such as the CG. It has been shown that 2P-FVM on adaptive meshes produces better conditioned discrete systems compared to the discrete systems formed on uniform meshes.

(2) There are many porous media flow simulators that approximate fluxes by the 2P-FVM but on uniform meshes. In the presented work, we are also approximating flux by the same method. The biggest advantage of the presented computational technique is thatit can be easily incorporated into an existing simulator (given that it is using the 2P-FVM). The presented numerical work validates that such an implementation can improve the simulation capability of the simulator.

(3) On adaptive meshes and for problems with regularity $\mathbf{H}^{1+\gamma}$, we are observing the following convergence behaviour:

$$\|\mathbf{p} - \mathbf{p}_h\|_{L_2} \approx C \ \mathrm{DOF}^{-2/2},$$

$$\|\mathbf{p} - \mathbf{p}_h\|_{L_\infty} \approx C \ \mathrm{DOF}^{-1/2} \ \text{and} \ \|\mathbf{u} - \mathbf{u}_h\|_{L_2} \approx C \ \mathrm{DOF}^{-1/2}.$$

References

Aavatsmark, I. (2002), "An introduction to multipoint flux approximations for quadrilateral grids", *Comput. Geosci.*, Vol. 6 Nos 3/4, pp. 405-32.

Aziz, K. and Settari, A. (1979), *Petroleum Reservoir Simulations*, Applied Science Publishers, New York, NY, p. 28.

Cao, H. (2002), "Development of techniques for general purpose simulators", PhD thesis, Stanford University, Stanford, CA.

Chen, Z. and Dai, S. (2002), "On the efficiency of adaptive finite element methods for elliptic problems with discontinuous coefficients", *SIAM J. Sci. Comput.*, Vol. 24, pp. 443-62.

Eclipse (1997), "Eclipse 100 technical description", Schlumberger Geoquest, Report.

Eigestad, G. and Klausen, R. (2005), "On the convergence of the multi-point flux approximation O-method: numerical experiments for discontinuous permeability", *Numerical Methods for Partial Differential Equations*, Vol. 21 No. 6, pp. 1079-98.

Ewing, R., Lazarov, R. and Vassilevski, P. (1991a), "Local refinement techniques for elliptic problems on cell-centered grids. I. Error analysis", *Math. Comp.*, Vol. 56 No. 194, pp. 437-61.

Ewing, R., Lazarov, R. and Vassilevski, P. (1991b), "Local refinement techniques for elliptic problems on cell-centered grids. III. Algebraic multilevel BEPS preconditioners", *Numer. Math.*, Vol. 59 No. 5, pp. 431-52.

Forsyth, P. Jr and Sammon, P. (1988), "Quadratic convergence for cell-centered grids", *Appl. Numer. Math.*, Vol. 4 No. 5, pp. 377-94.

Garcia, J. and Pruess, K. (2000), "Local grid refinement for multi-scale geothermal reservoir simulation with tough2", Technical Report LBNL-45646, Lawrence Berkeley National Laboratory, Berkeley, CA.

Garrido, I., Øian, E., Chaib, M., Fladmark, G.E. and Espedal, M.S. (2004), "Implicit treatment of compositional flow", *Comput. Geosci.*, Vol. 8 No. 1, pp. 1-19.

Hermitte, T. and Guerillot, D. (1993), "A more accurate numerical scheme for locally refined meshes in heterogeneous reservoirs", SPE 25261, pp. 321-31.

Hydro (2001), Norsk Hydro Research Center. First Reference Manual. Internal technical description.

Lee, S., Tchelepi, H. and DeChant, L. (1999), "Implementation of a flux-continuous finite difference method for stratigraphic, hexahedron grids. SPE 51901", *SPE Journal*, Vol. 7 No. 3, pp. 267-77.

Morin, P., Nochetto, R.H. and Siebert, K.G. (2000), "Data oscillation and convergence of adaptive FEM", *SIAM J. Numer. Anal.*, Vol. 38 No. 2, pp. 466-88, (electronic).

Nordbotten, J. and Eigestad, G. (2005), "Discretization on quadrilateral grids with improved monotonicity properties", *J. Comput. Phys.*, Vol. 203 No. 2, pp. 744-60.

Pruess, K. and Garcia, J. (2000), "A systematic approach to local grid refinement in geothermal reservoir simulation", *Proceedings of the World Geothermal Congress 2000, Kyushu-Tohoku, Japan, May, 28*, pp. 2809-14.

Pruess, K., Garcia, J., Kovscek, T., Oldenburg, C., Rutqvist, J., Steefel, C. and Xu, T. (2002), "Intercomparison of numerical simulation codes for geologic disposal of CO2", (LBNL-51813).

Riviere, B. (2000), "Discontinuous Galerkin finite element methods for solving the miscible displacement problem in porous media", PhD thesis, The University of Texas, Austin, TX.

Strang, G. and Fix, G. (1973), *An Analysis of the Finite Element Method*, Vol. 1, Wiley, New York, NY.

Süli, E. (1991), "Convergence of finite volume schemes for Poisson's equation on nonuniform meshes", *SIAM J. Numer. Anal.*, Vol. 28 No. 5, pp. 1419-30.

Verfürth, R. (1994), "A posteriori error estimation and adaptive mesh-refinement techniques", *Proceedings of the Fifth International Congress on Computational and Applied Mathematics*, Vol. 50, pp. 67-83, (Leuven, 1992).

Vorst, H.v.d. (2003), *Iterative Krylov Methods for Large Linear Systems*, in Cambridge monographs on applied and computational mathematics, Cambridge University Press, New York, NY.

Weiser, A. and Wheeler, M. (1988), "On convergence of block-centered finite differences for elliptic-problems", *SIAM J. Numer. Anal.*, Vol. 25 No. 2, pp. 351-75.

Wu, X. and Parashkevov, R. (2005), "Effect of grid deviation on flow solutions", SPE 92868.

Corresponding author
Sanjay Kumar Khattri can be contacted at: sanjay.khattri@gmail.com